

A DNA repair disorder caused by *de novo* monoallelic *DDB1* variants is associated with a neurodevelopmental syndrome

Susan M. White,^{1,2,*} Elizabeth Bhoj,³ Christoffer Nellåker,^{4,5,6} Augusta M.A. Lachmeijer,⁷ Aren E. Marshall,⁸ Kym M. Boycott,⁸ Dong Li,³ Wendy Smith,⁹ Taila Hartley,⁸ Arran McBride,⁸ Michelle E. Ernst,^{10,11} Alison S. May,¹² Dagmar Wieczorek,¹³ Rami Abou Jamra,¹⁴ Margarete Koch-Hogrebe,¹⁵ Katrin Öunap,^{16,17} Sander Pajusalu,^{16,17} K.L.I. van Gassen,⁷ Simon Sadedin,^{1,18} Sara Ellingwood,⁹ Tiong Yang Tan,^{1,2} John Christodoulou,^{2,19} Jaime Barea,²⁰ Paul J. Lockhart,^{2,19} Care4Rare Canada Consortium,⁸ Marjan M. Nezarati,²¹ and Kristin D. Kernohan^{8,22}

Summary

The DNA damage-binding protein 1 (DDB1) is part of the CUL4–DDB1 ubiquitin E3 ligase complex (CRL4), which is essential for DNA repair, chromatin remodeling, DNA replication, and signal transduction. Loss-of-function variants in genes encoding the complex components CUL4 and PHIP have been reported to cause syndromic intellectual disability with hypotonia and obesity, but no phenotype has been reported in association with *DDB1* variants. Here, we report eight unrelated individuals, identified through Matchmaker Exchange, with *de novo* monoallelic variants in *DDB1*, including one recurrent variant in four individuals. The affected individuals have a consistent phenotype of hypotonia, mild to moderate intellectual disability, and similar facies, including horizontal or slightly bowed eyebrows, deep-set eyes, full cheeks, a short nose, and large, fleshy and forward-facing earlobes, demonstrated in the composite face generated from the cohort. Digital anomalies, including brachydactyly and syndactyly, were common. Three older individuals have obesity. We show that cells derived from affected individuals have altered DDB1 function resulting in abnormal DNA damage signatures and histone methylation following UV-induced DNA damage. Overall, our study adds to the growing family of neurodevelopmental phenotypes mediated by disruption of the CRL4 ubiquitin ligase pathway and begins to delineate the phenotypic and molecular effects of DDB1 misregulation.

DNA integrity is essential for proper DNA function and, thus, human health. Preserving DNA integrity is difficult because many cell-intrinsic and cell-extrinsic factors cause thousands of damage events every day.¹ The DNA damage response signaling pathway maintains genome stability by sensing damage events and activating relevant DNA repair mechanisms.² *DDB1* (MIM: 60045) encodes the damage-specific DNA-binding protein 1, DDB1, which plays a vital role in the DNA damage response, specifically in the nucleotide excision repair pathway where it functions as part of the CUL4–DDB1 ubiquitin E3 ligase complex (CRL4).³ The CRL4 complex has also been found to function in other cellular processes, including regulation of chromatin remodeling, DNA replication, and signal transduction.^{4–8} Haploinsufficiency

of *CUL4B* (MIM: 300304) and *PHIP* (MIM: 612870), two additional CRL4 complex components, has been shown to lead to overlapping forms of syndromic intellectual disability. Pathogenic variants in *CUL4B* cause X-linked Cabezas syndrome (MIM: 300354), characterized by intellectual disability, seizures, brain malformations, behavioral issues, central obesity, macrocephaly, hypogonadotropic hypogonadism, and dysmorphic facial features.⁹ Pathogenic *PHIP* variants cause Chung-Jansen syndrome (MIM: 617991), characterized by intellectual disability, hypotonia, behavioral issues, obesity, and dysmorphic facial features.^{10,11}

Pathogenic *DDB1* variants have not yet been described in humans, although homologs of DDB1 have been shown as essential proteins in model organisms where

¹Victorian Clinical Genetics Services, Murdoch Children's Research Institute, Melbourne, VIC 3052, Australia; ²Department of Paediatrics, University of Melbourne, Melbourne, VIC 3010, Australia; ³Children's Hospital of Philadelphia, Philadelphia, PA 19104, USA; ⁴Nuffield Department of Women's and Reproductive Health, University of Oxford, Oxford OX3 9DU, UK; ⁵Institute of Biomedical Engineering, Department of Engineering Science, University of Oxford, Oxford OX3 7DQ, UK; ⁶Big Data Institute, Li Ka Shing Centre for Health Information and Discovery, University of Oxford, Oxford OX3 7LF, UK; ⁷Department of Genetics, Division Laboratories, Pharmacy and Biomedical Genetics, University Medical Center Utrecht, P.O. Box 85090, 3508 AB Utrecht, the Netherlands; ⁸Children's Hospital of Eastern Ontario Research Institute, University of Ottawa, Ottawa, ON K1H 8L1, Canada; ⁹Division of Genetics, Department of Paediatrics, Maine Medical Center, Portland, ME 04012, USA; ¹⁰Institute for Genomic Medicine, Columbia University Irving Medical Center, New York, NY 10032, USA; ¹¹Department of Genetics and Development, Columbia University Irving Medical Center, New York, NY 10032, USA; ¹²Division of Child Neurology, Department of Neurology, Columbia University Irving Medical Center, New York, NY 10032, USA; ¹³Institut für Human-genetik, Universitätsklinikum Düsseldorf, Heinrich-Heine-Universität Düsseldorf, Düsseldorf 40225, Germany; ¹⁴Institute of Human Genetics, University Medical Center Leipzig, Leipzig 04103, Germany; ¹⁵Vestische Kinder- und Jugendklinik Datteln, Universität Witten-Herdecke, Datteln 45711, Germany; ¹⁶Department of Clinical Genetics, United Laboratories, Tartu University Hospital, L. Puusepa 2, 51014 Tartu, Estonia; ¹⁷Department of Clinical Genetics, Institute of Clinical Medicine, University of Tartu, L. Puusepa 2, 51014 Tartu, Estonia; ¹⁸Program in Medical and Population Genetics, Broad Institute of MIT and Harvard, Boston, MA 01242, USA; ¹⁹Murdoch Children's Research Institute, Melbourne, VIC 3052, Australia; ²⁰Rady Children's Specialists of San Diego, San Diego, CA 92123, USA; ²¹North York General Hospital, Toronto, ON M2K 1E1, Canada; ²²Newborn Screening Ontario, Ottawa, ON K1H 8L1, Canada

*Correspondence: sue.white@vcgs.org.au
<https://doi.org/10.1016/j.ajhg.2021.03.007>

© 2021 American Society of Human Genetics.



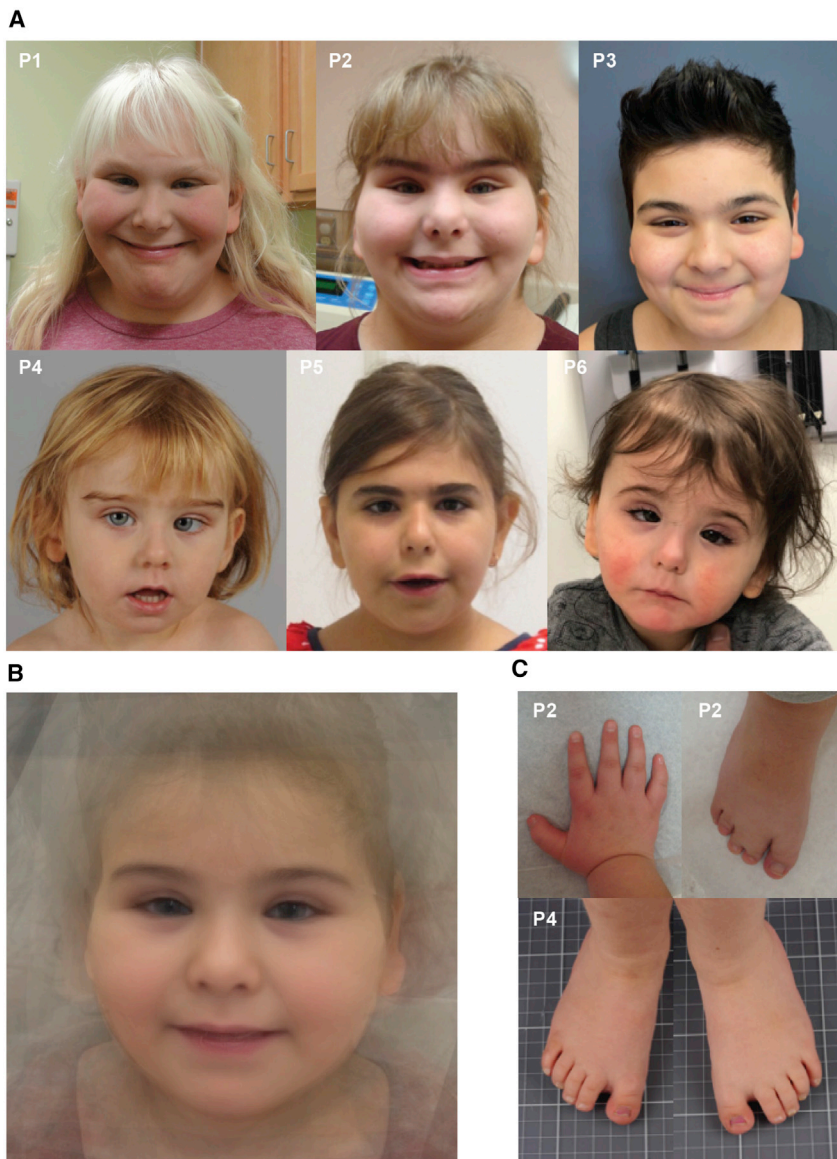


Figure 1. Face, hand, and feet and composite photographs

(A) Facial photographs of individuals 1, 2, 3, 4, and 5 showing horizontal eyebrows, short nose, and full cheeks.

(B) Composite image of individuals with *DDB1* variants showing key distinctive features of horizontal eyebrows, short nose, full cheeks, and large ear lobes.

(C) Photograph of hand in individual 2 showing brachydactyly and proximally placed thumb. Photograph of feet in individuals 2 and 4 showing syndactyly and brachydactyly.

All variants clustered within the first mono-functional DNA-alkylating methyl methanesulfonate (MMS1) domain of *DDB1* (Figure 2), and interestingly, we observed one recurrent protein change in four individuals, c.637G>A (GenBank: NM_001923.4) (p.Glu213Lys [GenBank: NP_001914.3]), and two different substitutions at the same residue, p.Arg188Trp and p.Arg188Gln. Each individual's data were submitted to Matchmaker Exchange with the *DDB1* variant's having been identified as a plausible disease candidate. Detailed phenotype comparison showed a strong clinical overlap, and this cohort of affected individuals was assembled (Table 1). Consistent features were hypotonia (7/8 individuals) and mild-moderate developmental delay or intellectual disability (8/8 individuals). Growth was variable. Two individuals had weight over the 97th centile and all three older individuals had a BMI in the obese range for their age. Malformations occurred in six individuals and included renal (2/8), cardiac (1/8), and anorectal malformations (2/8) and craniosynostosis (1/8). Brachydactyly was common and most noticeable in the feet (6/8 individuals), and two individuals had cutaneous toe syndactyly. Using photographs from the cohort, we generated a composite face.¹⁵ This illustrated the key dysmorphic features: horizontal or slightly bowed eyebrows, which were dark in two individuals with fair scalp hair; mild narrowing of the palpebral fissures; full cheeks; a short nose; and large, fleshy and forward-facing ear lobes (Figure 1; see supplemental notes and Table S4 for more detailed phenotypic information).

tissue-specific and global absence of the protein in mice and zebrafish often results in embryonic lethality, but no gross phenotype was observed for heterozygous knockout mice within the first year of life.^{12–14}

Therefore, it is likely that *DDB1* is also an essential gene, and pathogenic variants may cause a human phenotype resembling those of *CUL4B*- and *PHIP*-related conditions.

Herein, we present eight unrelated individuals (Figure 1) with *de novo* heterozygous *DDB1* variants. Because each of the affected individuals was an isolated case in their family, they were predicted to have either a *de novo* or recessive condition and exome/genome sequencing was performed at their respective genetics centers. Assessment of all potential recessive or *de novo* variants for each affected individual was conducted and a list of candidate variants for each individual is provided in Table S2. Each individual harbored a *de novo* monoallelic *DDB1* variant, each of which was predicted to be likely deleterious (Table S3).

An assessment of gnomAD showed that *DDB1* is missense- and CNV-depleted ($Z = 5.67$ and 1.30 , respectively) and intolerant to LoF variants (pLI = 1.0, o/e = 0.13 [0.08–0.24]). Eukaryotic homologs of *DDB1* were aligned, and conservation among the sequences is quite

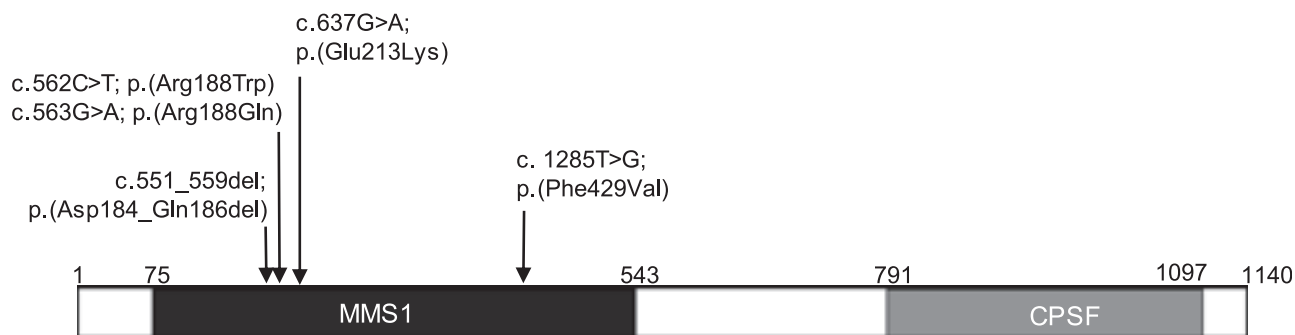


Figure 2. Protein domains of DDB1 and *de novo* variants found in affected individuals

DDB1 contains the MMS1 and CPSF protein domains. The MMS1 domain is homologous to the N-terminal region of MMS1; the protein itself protects against replication-dependent DNA damage in *Saccharomyces cerevisiae* and belongs to the DDB1 family of CUL4 adaptors. The function of the CPSF domain, homologous to the C terminus of the CPSF A subunit, is unknown but may be involved in RNA/DNA binding. All eight individuals had one *de novo* DDB1 missense variant, all of which were located within the coding region of the MMS1 domain and are listed above the schematic. Numbers above the schematic denote amino acid positions.

high, notably including the residues of interest in the affected individuals, which further demonstrates conservation of these sites (Figure S1C). Given the highly similar phenotype observed in these individuals with *de novo* apparently deleterious variants in what appears to be an essential protein, DDB1 represented a strong candidate gene for the observed phenotypes.

All DDB1 variants were missense, excepting the deletion found in individual 1. To assess the impact of the DNA deletion at the intron 4-exon 5 boundary found in individual 1, we performed splicing studies by using lymphoblasts from individual 1. This revealed a deletion of nucleotides c.551_559 within the transcript, corresponding to p.Asp184_Gln186del, and immunoblot analysis demonstrated no noticeable change in protein levels as a result (Figures S1A and S1B). On the basis of this result, it is not clear whether this variant is a gain- or loss-of-function variant, similar to the other variants in the cohort.

As our cohort's variants consisted of several missense variants and one in-frame deletion in the MMS1 domain of DDB1, the mutation mechanism was unclear. To determine whether DDB1 was sensitive to dosage perturbation and associated with human phenotypes when deleted or duplicated, we interrogated the Decipher database for deletions or duplications of DDB1.¹⁶ No individuals were identified where haploinsufficiency for DDB1 was associated with a phenotype. One individual was identified with a maternally inherited duplication including the DDB1 gene and another individual had a *de novo* 134 Mb deletion including DDB1 along with many other genes. No further conclusions could be garnered from these observations.

We next sought to investigate DDB1 function in lymphoblasts from individuals 2 and 4. A key function of DDB1 is to recognize and bind to areas of UV-induced DNA damage. We began by evaluating DDB1 levels in lymphoblast cells from control and affected individuals under basal conditions, as well as following UV induction of DNA damage. All experiments were conducted with a minimum of three replicates with different controls, and

representative images are shown. Immunoblot analysis of total protein extracts and qPCR of mRNA showed somewhat variable levels of DDB1 before and after DNA damage, all of which were within the range observed in controls (Figures 3A, 3B, and S2A). We conclude that overall DDB1 mRNA and protein levels are not significantly altered in cells from affected individuals. On the basis of these analyses, however, we cannot distinguish whether mutant DDB1 is expressed equivalently to wild-type or whether there is compensation from the opposing allele.

To assess DNA damage signaling we began by measuring γ H2AX, a marker of DNA damage that localizes to double-stranded breaks. Cells were again treated with UV, and immunoblot analysis was conducted. We found that γ H2AX is induced in both control and affected lymphoblasts, as expected, but these levels are not sustained for as long after DNA damage in affected cells compared to controls. We next assessed a second marker of DNA damage response, phosphorylation of Thr68 on CHK2 (p-Thr68-CHK2), a protein kinase that functions in the cell cycle arrest and apoptosis pathways following DNA damage. As expected, p-Thr68-CHK2 was increased after UV exposure in all cells, but interestingly, these levels appear noticeably higher 1 h after DNA damage in both affected samples compared to control lymphoblasts (Figures 3A and S2A). These data suggest that the DNA damage response is altered in DDB1 cells from affected individuals. We next sought to investigate whether an altered DNA damage response affected growth of these cells. Cellular proliferation of the lymphoblast cells was assessed through cell counts at days 0–10, and we determined that the DDB1 variants do not cause altered lymphoblast proliferation rates compared to control (Figures 3C and S2B). Moreover, when cells were subjected to DNA damage by UV, despite differences in DNA damage signaling, no significant differences in proliferation were observed between control and affected lymphoblasts (Figures 3C and S2B).

Table 1. Phenotype information for individuals with DDB1 variants

Individual	P1	P2	P3	P4	P5	P6	P7	P8
Gender	female	female	male	female	female	male	male	female
Age at last assessment	17 y	9 y 2 m	10 y 8 m	3 y	13 y	22 m	2 y 11 m	1 y
Molecular data								
DDB1 variant (g) Hg19	chr11: 61094361_61094369del	chr11: 61094353G>A	chr11: 61094352C>T			chr11: 61094278C>T		chr11: 61083980A>C
DDB1 variant (c) (NM_001923.4) variant (p) (NP_001914.3)	c.551_559del (p.Asp184_Gln186del)	c.562C>T (p.Arg188Trp)	c.563G>A (p.Arg188Gln)			c.637G>A (p.Glu213Lys)		c.1285T>G (p.Phe429Val)
Phenotypic features								
Hypotonia	moderate	mild	nil	moderate	moderate	moderate	moderate	moderate
Intellectual disability	moderate	moderate DD	mild (IQ = 69)	mild	mild-moderate	mild	moderate DD	moderate DD
Craniofacial	thick, light-blonde eyebrows; deep-set, upslanting palpebral fissures; epicanthic folds; short nose in early childhood; very full cheeks; thin upper vermilion; wide mouth; large ears with large and long ear lobes	horizontal, dark eyebrows synophrys; long palpebral fissures with lateral extension; epicanthus inversus; long dark eyelashes; short nose; underdeveloped alae nasi; mid-face hypoplasia; full cheeks; low-set, large ears with long fleshy lobes	synophrys; short palpebral fissures; full cheeks; large earlobes	horizontal, dark eyebrows with medial broadening; lateral extension to palpebral fissures; short nose; mid-face hypoplasia; thin upper vermilion; large ears with fleshy lobes	dark, horizontal, heavy eyebrows; round face; mild midface hypoplasia; full cheeks; protruding upper lip; thin vermilion retrognathia asymmetric; occlusion of teeth; large fleshy ears and earlobes	medial broadening of eyebrows; telecanthus; lateral extension to palpebral fissures; epicanthus; long eyelashes; short nose, retrognathia; thin, tented upper vermilion; low set, fleshy ears	deep-set eyes; epicanthus; hypotelorism convergent strabismus; nystagmus; short and upturned nose; underdeveloped alae nasi; full cheeks; large, simple ears	medial broadening of eyebrows; telecanthus proptosis epicanthus inversus; flat nasal bridge; mid-face hypoplasia
Malformations	anterior anus and recto-vaginal fistula	accessory band across left ventricle of heart, horseshoe kidney, anterior ectopic anus, dysgenesis of corpus callosum	nil	nil	horseshoe kidney with left vesico-ureteric reflux, pelvicalyceal dilatation and megaureter	nil	mild left hydronephrosis	metopic cranio-synostosis
Hands and feet	small hands and feet, short fourth metacarpals, brachydactyly	2–3 toe syndactyly, brachydactyly	short toes	short toes	short toes	NR	2–3 toe partial syndactyly	NR
Other	joint laxity, ADHD, anxiety, hypothyroidism, recurrent otitis media, obesity	joint laxity, truncal obesity	frequent otitis media	mild joint laxity, bilateral hip dysplasia, obstructive sleep apnea	mild joint laxity	NR	gastro-esophageal reflux	NR

NR, not reported; DD, developmental delay.

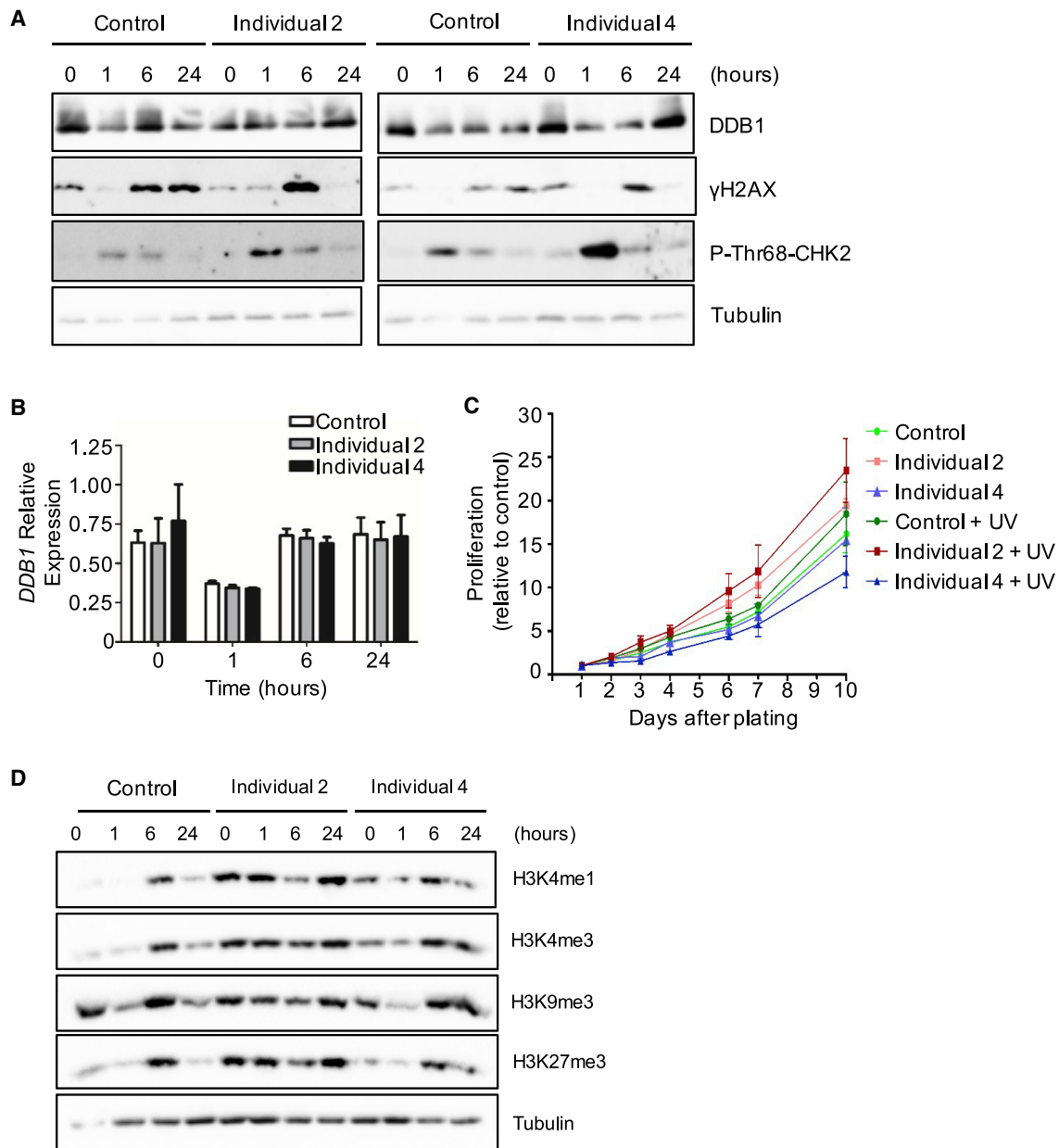


Figure 3. *DDB1* missense variants in lymphoblast cells result in altered DNA damage signatures and histone methylation following UV damage

(A) Immunoblot analysis on total extracts from control and affected lymphoblast cells. Untreated cells are shown at the 0 h time point, whereas the other time intervals indicate the number of h following UV exposure. Total *DDB1* and the levels of γ H2AX and p-Thr68-CHK2 phosphorylation were assessed: *DDB1* was found to be unchanged and γ H2AX and p-Thr68-CHK2 levels were induced as expected, p-Thr68-CHK2 to a higher level than controls and γ H2AX to a similar level as controls but was not sustained.

(B) Real-time PCR analysis on extracts from lymphoblast cells showing transcript levels of *DDB1* before and after UV exposure are similar between cells from affected individuals and control individuals.

(C) Cell proliferation of control and affected lymphoblast cells was measured by harvesting and counting cells on each of the specified days after initial plating, either with or without UV exposure.

(D) Immunoblot analysis of total extracts from control and affected lymphoblast cells. Untreated cells are shown at the 0 h time point, whereas the other time intervals indicate the number of h following UV exposure. Levels of various histone H3 methylations were assessed and found to be abnormal in cells from affected individuals. Immunoblots in this figure are representative images of at least three biological replicates, and graphed data represent the mean of three biological replicates; error bars depict standard error of the mean.

Given the altered DNA damage signaling in cells from affected individuals, we hypothesized that other *DDB1*-regulated pathways may also be affected. The *CUL4-DDB1* complexes interact with multiple WD40-repeat proteins, including *WDR5* and the Polycomb-group protein

EED, which are core components of histone methylation complexes necessary for histone H3 methylation at K4 or K27, respectively.^{4,17,18} More recently, it has also been shown that *DDB1*- and *CUL4*-associated factor 8 (*DCAF8*), another WD40-repeat protein, interacts with

CRL4 to ubiquitinate H3 in adult mouse hepatocytes, which promotes methylation of H3K9.¹⁹ Because of these associations between H3 methylation and WD40-repeat proteins that interact with CRL4, we investigated whether there were any changes in H3K4, H3K9, and H3K27 methylation in cells from affected individuals. H3K27me3 did not seem to be affected by *DDB1* variants, as levels were increased at 6 h and 24 h after UV exposure in both control and lymphoblast cells from affected individuals (Figures 3D and S2C). The general trend for H3K4me1, H3K4me3, and H3K9me3 was increased levels at 6 h after DNA damage in control lymphoblasts, which start to return to basal levels after 24 h (Figures 3D and S2C). In both affected lymphoblast cells, H3K4me1 and H3K4me3 protein levels appeared to be increased compared to control cells without induction of DNA damage. H3K4 and H3K9 methylation in affected lymphoblasts were then increased later than in the control after UV exposure, sometimes beginning 6 h after UV and generally elevated 24 h after treatment as well. However, the increase in these histone modifications in lymphoblasts from affected individuals following DNA damage was sometimes subtle because of the abundance of these marks at baseline. Together, these results suggest that increased histone methylation may occur later and may also be sustained for longer periods of time following UV exposure in cells from affected individuals (Figure 3D). Given the abnormal *DDB1* downstream effects, and the identification of eight individuals with a highly similar phenotype, we conclude that we have identified a unique condition caused by monoallelic *de novo* variants in the MMS1 domain of *DDB1*.

DDB1 functions in a complex with CUL4 and PHIP. Loss-of-function variants in genes encoding these proteins, *CUL4B* and *PHIP*, have been observed in individuals with syndromic intellectual disability. This suggests a common pathogenic mechanism for this family of phenotypes.^{9,10} Seven of the eight individuals in this have missense variants in *DDB1*, including one recurrent protein change, p.Glu213Lys, and two different substitutions at the same amino acid residue (p.Arg188Trp and p.Arg188Gln), while the remaining variant is an in-frame deletion of three amino acids. This suggests these may function through a dominant negative or gain-of-function mechanism, although loss-of-function cannot be excluded.

Data from a recent study investigating regional missense variant constraint demonstrate that the *DDB1* transcript has two distinct sub-genic regions, both of which are observed to contain less than half of the expected number of missense variants and together span the entire gene.²⁰ Interestingly, transcripts and regions of transcripts that have the fraction of expected variation observed as ≤ 0.6 represent 14% of the coding region of the human genome but contain 89% of all the ClinVar pathogenic missense variants.²⁰ Therefore, it remains a possibility that because the entire *DDB1* transcript is depleted of missense variants, var-

iants outside of the MMS1 domain may still have yet to be identified as contributing to this neurodevelopmental disorder. This is further supported by the fact that the majority of *DDB1* is comprised of three WD40 β -propeller structures; the affected residues Asp184 to Glu213 are all present in one of them, Phe429 is present in the second, while the third remaining WD40 β -propeller overlaps the CPSF domain.²¹ Because WD40 β -propellers have no catalytic activity and instead function together as protein-protein or protein-DNA interaction platforms, alterations within these regions most likely impact a number of overlapping *DDB1* interactions.²² Although the functional studies showed clear effects downstream of *DDB1*, it was not possible to discern a mutational mechanism. For the variants p.Asp184_Gln186del, p.Arg188Gln, and p.Phe429Val, present in individuals 1, 3, and 8, respectively, no functional studies were able to be undertaken because cells were not available. Nevertheless, the phenotypic similarity across the cohort led us to conclude that the rare, deleterious *DDB1* variants in individuals 1, 3, and 8 were also highly likely to be pathogenic. Phenotypic features in common across the *CUL4B*-, *PHIP*-, and *DDB1*-related conditions include intellectual disability and obesity, and there is some intriguing similarity in the facial dysmorphism of all three phenotypes and digital features in the *CUL4B*- and *DDB1*-related phenotypes.^{9–11} In contrast to our cohort, brain malformations, tremor, macrocephaly, and hypogonadotropic hypogonadism are common features in Cabezas syndrome and behavioral issues are frequently reported for both Cabezas and Chung-Jansen syndromes.

The common phenotype of obesity is interesting because there is growing evidence linking the CRL4 complex with control of adipogenesis. *WDT1*, which is known to suppress adipogenesis, is a member of the CRL4 complex. Obesity is observed in humans and mice when expression of *WDT1* is reduced.^{23–25} Moreover, disruption of the interaction between *WDT1* and *DDB1* *in vitro* leads to adipogenic gene expression.²⁶ The CRL4 complex also has a role in the regulation of glucose metabolism, promoting hepatic gluconeogenesis.²⁷ Of interest, one individual in our study had hypoglycemia in the neonatal period, and it is therefore possible that the *DDB1* variant in this individual adversely affected the control of glucose homeostasis.

DDB1 and *DDB2* form the UV-DDB complex, which is integral to the nucleotide excision repair process.³ Biallelic variants in *DDB2* (MIM: 600811) cause xeroderma pigmentosum group E (MIM: 278740), a neurocutaneous syndrome causing skin cancers and dermatological and ocular features.²⁸ Although *DDB1* is a protein involved in DNA repair, we did not observe the cardinal phenotypes seen in DNA repair disorders, such as growth restriction, skin alterations, premature aging, and a predisposition to malignancy. In addition, most DNA repair disorders are caused by bi-allelic loss-of-function variants. These findings further support a dominant negative or gain-of-function mechanism for the *DDB1* variants in this study or

could be explained by an additional yet unknown function for DDB1. In lymphoblasts from affected individuals from our study, we find altered DNA damage signaling through changes in γ H2AX and Chk2 phosphorylation, consistent with DDB1's playing an important role in repair following UV damage. Somatic *DDB1* variants are reported in breast, lung, and gastrointestinal malignancies, and the CRL4 complex demonstrates aberrant function in many different malignancies.²⁹ Interestingly, within the Catalogue Of Somatic Mutations In Cancer (COSMIC), missense variants at the Arg188 residue are found in nine samples, making it the most frequently affected amino acid of DDB1.²⁹ Of the samples in COSMIC with missense variants at the Arg188 residue, p.Arg188Trp is one of the nine and p.Arg188Gln represents another five, although neither of these variants were studied to determine their functional impact, so it is unclear whether DDB1 acts primarily as a tumor suppressor or oncogene in these contexts. Although there is no cancer involvement in the cohort described here, this may represent yet another gene family in which germline variants cause a neurodevelopmental phenotype and somatic variants cause cancer.^{29,30}

In summary, we have used genomic sequencing to identify *de novo* variants in *DDB1* in eight unrelated individuals with overlapping phenotypes of intellectual disability and hypotonia with a facial gestalt of maxillary hypoplasia, small nose, lateral extension of the palpebral fissures, and straight eyebrows. Functional characterization in cells from affected individuals showed altered DDB1 function resulting in abnormal DNA damage signatures and histone methylation following UV-induced DNA damage. Our findings extend the disease association of components of the CRL4 and UV-DDB complexes, inform the phenotypic understanding of this disorder, and provide insight into the molecular pathogenesis of this condition.

Data and code availability

There are restrictions to the availability of genomic sequencing data in this project because of consent limitations.

Supplemental information

Supplemental information can be found online at <https://doi.org/10.1016/j.ajhg.2021.03.007>.

Acknowledgments

The authors would like to thank the individuals and their families for their generous participation in this and the many healthcare providers involved in their care. We thank Natalie Tan for her assistance with the photographic figure. Funding for the UDP-Vic was provided by philanthropic donation and the Murdoch Children's Research Institute. The research conducted at the Murdoch Children's Research Institute was supported by the Victorian Government's Operational Infrastructure Support Program,

the Harbig Family Foundation, and The Royal Children's Hospital Foundation. This work was supported, in part, by the Care4Rare Canada Consortium funded by Genome Canada and the Ontario Genomics Institute (OGI-147), the Canadian Institutes of Health Research, Ontario Research Fund, Genome Alberta, Genome British Columbia, Genome Quebec, and Children's Hospital of Eastern Ontario Foundation. Sequencing and analysis was provided by the Broad Institute of MIT and Harvard Center for Mendelian Genomics (Broad CMG) and was funded by the National Human Genome Research Institute, the National Eye Institute, and the National Heart, Lung, and Blood Institute grant UM1HG008900 to Daniel MacArthur and Heidi Rehm. Research reported in this publication was supported by the National Human Genome Research Institute of the National Institutes of Health under award number U01HG009599. The content is solely the responsibility of the authors and does not necessarily represent the official views of the National Institutes of Health. P.J.L. is supported by the Vincent Chiodo Foundation. D.W. and K.Ö. are members of the European Reference Network ITHACA. K.Ö. and S.P. were supported by Estonian Research Council grants PRG471, MOBTP175, and PUTJD827.

Declaration of interests

The authors declare no competing interests.

Received: October 26, 2020

Accepted: March 2, 2021

Published: March 19, 2021

Web resources

GenBank, <https://www.ncbi.nlm.nih.gov/genbank/>
Genome Aggregation Database (gnomAD), <https://gnomad.broadinstitute.org/>
Matchmaker Exchange, <https://www.matchmakerexchange.org/>
OMIM, <https://omim.org/>

References

1. Tiwari, V., and Wilson, D.M., 3rd. (2019). DNA Damage and Associated DNA Repair Defects in Disease and Premature Aging. *Am. J. Hum. Genet.* *105*, 237–257.
2. Maréchal, A., and Zou, L. (2013). DNA damage sensing by the ATM and ATR kinases. *Cold Spring Harb. Perspect. Biol.* *5*, a012716.
3. Scrima, A., Koníčková, R., Czyzewski, B.K., Kawasaki, Y., Jeffrey, P.D., Groisman, R., Nakatani, Y., Iwai, S., Pavletich, N.P., and Thomä, N.H. (2008). Structural basis of UV DNA-damage recognition by the DDB1-DDB2 complex. *Cell* *135*, 1213–1223.
4. Higa, L.A., Wu, M., Ye, T., Kobayashi, R., Sun, H., and Zhang, H. (2006). CUL4-DDB1 ubiquitin ligase interacts with multiple WD40-repeat proteins and regulates histone methylation. *Nat. Cell Biol.* *8*, 1277–1283.
5. Nishitani, H., Sugimoto, N., Roukos, V., Nakanishi, Y., Saijo, M., Obuse, C., Tsurimoto, T., Nakayama, K.I., Nakayama, K., Fujita, M., et al. (2006). Two E3 ubiquitin ligases, SCF-Skp2 and DDB1-Cul4, target human Cdt1 for proteolysis. *EMBO J.* *25*, 1126–1136.
6. Ghosh, P., Wu, M., Zhang, H., and Sun, H. (2008). mTORC1 signaling requires proteasomal function and the involvement of CUL4-DDB1 ubiquitin E3 ligase. *Cell Cycle* *7*, 373–381.

7. Hrecka, K., Gierszewska, M., Srivastava, S., Kozaczekiewicz, L., Swanson, S.K., Florens, L., Washburn, M.P., and Skowronski, J. (2007). Lentiviral Vpr usurps Cul4-DDB1[VprBP] E3 ubiquitin ligase to modulate cell cycle. *Proc. Natl. Acad. Sci. USA* *104*, 11778–11783.
8. Tong, X., Zhang, D., Guha, A., Arthurs, B., Cazares, V., Gupta, N., and Yin, L. (2015). CUL4-DDB1-CDT2 E3 Ligase Regulates the Molecular Clock Activity by Promoting Ubiquitination-Dependent Degradation of the Mammalian CRY1. *PLoS ONE* *10*, e0139725.
9. Vulto-van Silfhout, A.T., Nakagawa, T., Bahi-Buisson, N., Haas, S.A., Hu, H., Bienek, M., Vissers, L.E.L.M., Gilissen, C., Tzschach, A., Busche, A., et al. (2015). Variants in CUL4B are associated with cerebral malformations. *Hum. Mutat.* *36*, 106–117.
10. Webster, E., Cho, M.T., Alexander, N., Desai, S., Naidu, S., Bekheirnia, M.R., Lewis, A., Retterer, K., Jussola, J., and Chung, W.K. (2016). De novo PHIP-predicted deleterious variants are associated with developmental delay, intellectual disability, obesity, and dysmorphic features. *Cold Spring Harb. Mol. Case Stud.* *2*, a001172.
11. Jansen, S., Hoischen, A., Coe, B.P., Carvill, G.L., Van Esch, H., Bosch, D.G.M., Andersen, U.A., Baker, C., Bauters, M., Bernier, R.A., et al. (2018). A genotype-first approach identifies an intellectual disability-overweight syndrome caused by PHIP haploinsufficiency. *Eur. J. Hum. Genet.* *26*, 54–63.
12. Cang, Y., Zhang, J., Nicholas, S.A., Bastien, J., Li, B., Zhou, P., and Goff, S.P. (2006). Deletion of DDB1 in mouse brain and lens leads to p53-dependent elimination of proliferating cells. *Cell* *127*, 929–940.
13. Cang, Y., Zhang, J., Nicholas, S.A., Kim, A.L., Zhou, P., and Goff, S.P. (2007). DDB1 is essential for genomic stability in developing epidermis. *Proc. Natl. Acad. Sci. USA* *104*, 2733–2737.
14. Hu, Z., Holzschuh, J., and Driever, W. (2015). Loss of DDB1 Leads to Transcriptional p53 Pathway Activation in Proliferating Cells, Cell Cycle Deregulation, and Apoptosis in Zebrafish Embryos. *PLoS ONE* *10*, e0134299.
15. Reijnders, M.R.E., Miller, K.A., Alvi, M., Goos, J.A.C., Lees, M.M., de Burca, A., Henderson, A., Kraus, A., Mikat, B., de Vries, B.B.A., et al.; Deciphering Developmental Disorders Study (2018). De Novo and Inherited Loss-of-Function Variants in TLK2: Clinical and Genotype-Phenotype Evaluation of a Distinct Neurodevelopmental Disorder. *Am. J. Hum. Genet.* *102*, 1195–1203.
16. Firth, H.V., Richards, S.M., Bevan, A.P., Clayton, S., Corpas, M., Rajan, D., Van Vooren, S., Moreau, Y., Pettett, R.M., and Carter, N.P. (2009). DECIPHER: Database of Chromosomal Imbalance and Phenotype in Humans Using Ensembl Resources. *Am. J. Hum. Genet.* *84*, 524–533.
17. Simon, J.A., and Kingston, R.E. (2009). Mechanisms of polycomb gene silencing: knowns and unknowns. *Nat. Rev. Mol. Cell Biol.* *10*, 697–708.
18. Wysocka, J., Swigut, T., Milne, T.A., Dou, Y., Zhang, X., Burlingame, A.L., Roeder, R.G., Brivanlou, A.H., and Allis, C.D. (2005). WDR5 associates with histone H3 methylated at K4 and is essential for H3 K4 methylation and vertebrate development. *Cell* *121*, 859–872.
19. Li, G., Ji, T., Chen, J., Fu, Y., Hou, L., Feng, Y., Zhang, T., Song, T., Zhao, J., Endo, Y., et al. (2017). CRL4^{DCAF8} Ubiquitin Ligase Targets Histone H3K79 and Promotes H3K9 Methylation in the Liver. *Cell Rep.* *18*, 1499–1511.
20. Samochoa, K.E., Kosmicki, J.A., Karczewski, K.J., O'Donnell-Luria, A.H., Pierce-Hoffman, E., MacArthur, D.G., Neale, B.M., Mark, J., and Daly, M.J. (2017). Regional missense constraint improves variant deleteriousness prediction. *bioRxiv*. <https://doi.org/10.1101/148353>.
21. UniProt Consortium (2019). UniProt: a worldwide hub of protein knowledge. *Nucleic Acids Res.* *47* (D1), D506–D515.
22. Xu, C., and Min, J. (2011). Structure and function of WD40 domain proteins. *Protein Cell* *2*, 202–214.
23. Galgani, J.E., Kelley, D.E., Albu, J.B., Krakoff, J., Smith, S.R., Bray, G.A., Ravussin, E.; and Look AHEAD Adipose Research Group (2013). Adipose tissue expression of adipose (WDT1) gene is associated with lower fat mass and enhanced insulin sensitivity in humans. *Obesity (Silver Spring)* *21*, 2244–2248.
24. Lai, C.-Q., Parnell, L.D., Arnett, D.K., García-Bailo, B., Tsai, M.Y., Kabagambe, E.K., Straka, R.J., Province, M.A., An, P., Borocki, I.B., et al. (2009). WDT1, the ortholog of Drosophila adipose gene, associates with human obesity, modulated by MUFA intake. *Obesity (Silver Spring)* *17*, 593–600.
25. Suh, J.M., Zeve, D., McKay, R., Seo, J., Salo, Z., Li, R., Wang, M., and Graff, J.M. (2007). Adipose is a conserved dosage-sensitive antiobesity gene. *Cell Metab.* *6*, 195–207.
26. Groh, B.S., Yan, F., Smith, M.D., Yu, Y., Chen, X., and Xiong, Y. (2016). The antiobesity factor WDT1 suppresses adipogenesis via the CRL4WDT1 E3 ligase. *EMBO Rep.* *17*, 638–647.
27. Tong, X., Zhang, D., Charney, N., Jin, E., VanDommelen, K., Stamper, K., Gupta, N., Saldade, J., and Yin, L. (2017). DDB1-mediated CRY1 degradation promotes FOXO1-driven gluconeogenesis in liver. *Diabetes* *66*, 2571–2582.
28. Tang, J., and Chu, G. (2002). Xeroderma pigmentosum complementation group E and UV-damaged DNA-binding protein. *DNA Repair (Amst.)* *1*, 601–616.
29. Tate, J.G., Bamford, S., Jubb, H.C., Sondka, Z., Beare, D.M., Bindal, N., Boutselakis, H., Cole, C.G., Creatore, C., Dawson, E., et al. (2019). COSMIC: the Catalogue Of Somatic Mutations In Cancer. *Nucleic Acids Res.* *47* (D1), D941–D947.
30. McDonnell, L.M., Kernohan, K.D., Boycott, K.M., and Sawyer, S.L. (2015). Receptor tyrosine kinase mutations in developmental syndromes and cancer: two sides of the same coin. *Hum. Mol. Genet.* *24* (R1), R60–R66.

Supplemental information

**A DNA repair disorder caused by *de novo*
monoallelic *DDB1* variants is associated with
a neurodevelopmental syndrome**

Susan M. White, Elizabeth Bhoj, Christoffer Nellåker, Augusta M.A. Lachmeijer, Aren E. Marshall, Kym M. Boycott, Dong Li, Wendy Smith, Taila Hartley, Arran McBride, Michelle E. Ernst, Alison S. May, Dagmar Wieczorek, Rami Abou Jamra, Margarete Koch-Hogrebe, Katrin Öunap, Sander Pajusalu, K.L.I. van Gassen, Simon Sadedin, Sara Ellingwood, Tiong Yang Tan, John Christodoulou, Jaime Barea, Paul J. Lockhart, Care4Rare Canada Consortium, Marjan M. Nezarati, and Kristin D. Kernohan

SUPPLEMENTAL NOTES

CASE REPORTS

Individual 1

Individual 1 is the oldest of three full siblings born to healthy, non-consanguineous parents of Northern European ancestry. Following a pregnancy that was complicated by fetal growth restriction, she was born at 38 weeks gestation via Cesarean section due to breech positioning, birth weight 2040g (<3rd centile). She was admitted to the neonatal intensive care unit for 10 days due to feeding issues requiring nasogastric tube feeding. A small rectovaginal fistula was treated with rectal dilation. Mild micrognathia was noted.

Brain MRI revealed a structurally unremarkable brain structure with mild dilatation of the third and lateral ventricles. A renal ultrasound was normal. Normal molecular testing has included a peripheral blood karyotype, methylation studies for Prader-Willi syndrome, Fragile-X analysis, subtelomeric FISH analysis, and FISH 22q11 microdeletion. Oligo-based chromosome microarray was normal in 2008. A multi-gene NextGeneration Panel for diagnoses (178 genes) associated with intellectual disability was non-diagnostic in 2016.

Developmental milestones were delayed: she sat at 11 months, began crawling at two years and walked with assistance at 2 years 10 months of age. She used signs and approximately 10 words by age 4 years 6 months. Her motor development was always ahead of her language/speech development. She had ongoing issues with feeding, with sensitivity to textures. She received Early Intervention Services and Specialized Education (functional life skills programming in public school).

Her medical issues have included hypothyroidism; initial myopia with strabismus now with normal vision; constipation; recurrent urinary tract infections; gastroesophageal reflux;

increased cholesterol (diet controlled); recurring otitis media; ADHD, anxiety; overweight/obesity and short stature.

Her length/height were at the 10th percentile until 24 months of age when her height crossed percentiles. It then remained consistently at the 2nd centile. Her weight was less than the 50th centile in infancy, and between the 50-75th centile in childhood until puberty when her weight continued to increase and her height remained stable.

At her most recent evaluation, she was 18 years old and in overall good health. She continued to be treated for hypothyroidism and easily develops middle ear fluid. She attended school in a functional life skills classroom with occupational therapy, physical therapy, and speech therapy. She had a behavioural support staff for 12 hours per week. Height was 149.4 cm (2nd centile) and weight 87.2.kg (97th centile), BMI 39.2 (95-97th centile, obese range).

Examination was notable for being very interactive and expressive, but with few words. She had very full cheeks and a small midface, round facies, deeply set eyes with bilateral epicanthus. The neck was short with a prominent posterior fullness. Brachydactyly of the upper and lower extremities was present with short fourth metacarpals bilaterally. She had a very fair complexion and short, thin and upturned toe nails.

Individual 2

Individual 2 is the youngest of three children to healthy non-consanguineous parents of Ashkenazi Jewish ancestry. She was born at 40 weeks by a spontaneous vaginal delivery. She had neonatal hypoglycaemia and tachypnea and required neonatal intensive care admission for one month, at which time mild hypotonia, dysgenesis of the corpus callosum, mild ventriculomegaly, horseshoe kidney and anterior ectopic anus. She developed significant

hearing loss requiring hearing aides. Development was globally delayed and she did not begin communicating with words until approximately age 3. She began walking independently at age 2.

When assessed aged 6 ½ years, she had ~30 words, nasal speech but excellent receptive language in Russian and English. She was able to dress and undress independently. She had ongoing issues with balance, did not climb structures, but was able to climb stairs with alternate feet with support. She was on prophylactic antibiotics to prevent urinary tract infections.

At 6 ½ years, her head circumference measured 53.5cm (50-98th centile), weight 36.6kg (>98th centile), and height 120cm (50th centile). At age nine years, weight was 52.7kg (>97th centile) and height 137cm (75th centile), BMI 28.2 (95-97th centile, obese range).

She had fair blond hair with noticeably darker eyebrows with synophrys. Her eyes were a striking blue/cobalt color and displayed epicanthus inversus. She had a short nose with small nares and underdeveloped alae nasi, a narrow base and a prominent nasal bridge. The ears were mildly low-set. She had a short neck, a normally shaped chest and slightly prominent fibro-fatty deposition on the lateral dorsal aspect of the torso. The skin overlying this area was noticeably denser. She had a hirsute back with fine vellous hairs. There was significant partial cutaneous syndactyly of the 2nd-3rd toes bilaterally. She had short fingers, clinodactyly of the 5th fingers, proximally placed thumbs and fetal finger pads. She had mild hypotonia but brisk reflexes and hypermobility of the joints.

Individual 3

Individual 3 is the second of two children to healthy unrelated parents of Turkish origin. He was born after an uneventful pregnancy per Cesarean section at 42 weeks' gestation, birth

weight 4.04kg (70th centile), length 54cm (60th centile) and head circumference 37cm (74th centile). Feeding and muscle tone were normal. He was not able to cry loudly. Sitting without support was possible at twelve months and walking at 19 months. Speech was not delayed with first words at ten months. He had recurrent otitis media, he was a quiet and happy baby.

Assessment at age 10 ½ years showed mild motor and mild speech delay with good social skills. He was able to read simple children books, he was able to write his name and can calculate similar to a six-year-old child. He spoke complex sentences in Turkish and German. Weight was > 97th centile, height on the 95th centile and head circumference on the 79th centile, BMI 27.8 (95-97th centile, obese range).

He had a low frontal hairline, thick and slightly bowed eyebrows with synophrys and large ears with large and forward-facing earlobes. His hands were large with tapering fingers.

Individual 4

Individual 4 is the second of three children to healthy unrelated parents of Anglo-Australian background. She was born after an uneventful pregnancy at 42 weeks' gestation, birth weight 3.48kg (70th centile), length 52cm (93rd centile) and head circumference 34.5cm (60th centile). She had significant hypotonia in infancy, sitting at fourteen months and walking at 2 years, three months. Speech was mildly delayed with first words at fifteen months. She had a strabismus for which she wears glasses and audiology showed conductive hearing loss treated with tympanostomy tubes. She had an adenotonsillectomy for obstructive sleep apnoea.

Assessment at age three years showed moderate motor and mild speech delay with good social skills. Weight was on the 14th centile, height on the 15th centile and head circumference on the 10th centile. She had marked facial hypotonia with an open-mouthed expression, fair scalp hair with dark eyebrows which were horizontal, thick and had a medial flare and lateral extension. She had long eyelashes and her palpebral fissures had a lateral extension. She had large fleshy ears and earlobes. She had short toes. She had soft skin. Clinically, a diagnosis of Congenital Disorders of Glycosylation was considered because of the marked hypotonia. Renal ultrasound and echocardiogram were normal. Brain MRI aged 13 months was normal.

Individual 5

Individual 5 is the second child of Armenian non-consanguineous parents. At the age of 9 years she and her family arrived in the Netherlands. Not much information is available on her early development but she was born at a gestational age of 36 weeks with a birth weight of 2900 grams (25-50th centile) and her birth length was 47 cm (50th centile). Neonatal feeding difficulties and jaundice were reported. Assessment at age 13 showed a friendly girl with a mild to moderate psychomotor retardation, truncal obesity, a low anterior hairline, horizontal thick eyebrows, hirsutism, large fleshy ears and earlobes, small hands and feet and her height was below her target height (height -3.6 SDS, target height - 1.55 SD). She was diagnosed with a horseshoe kidney and uterine septum. She underwent nephrectomy of the left side of her horseshoe kidney because of reflux mediated nephropathy, recurrent urinary infections and hypertension. A correction of the urethral meatus and a resection of a vaginal septum were performed. A congenital bicornuate uterus was identified. Clinically, a diagnosis of Cornelia de Lange syndrome was considered based

on her features. Previously performed karyotyping showed a normal karyotype, DNA-diagnostics by Sanger sequencing in Cornelia de Lange syndrome associated genes (*NIPBL*, *SMC1A* and *HDAC8*) showed no abnormalities and a SNP-array showed a normal female profile.

Individual 6

Individual 6 was conceived via IVF and is the first liveborn child to healthy Caucasian parents. Oligohydramnios was noted at 38.3 weeks and he was born via scheduled Cesarean section. He had a NICU stay for 10 days, mainly for temperature instability and glucose instability. He was diagnosed with torticollis while in the NICU. Within a month he had failure to thrive, but growth recovered after being switched to formula. He had gross developmental delay, mild intellectual disability and hypotonia. Mild dysmorphism included low set ears, epicanthal folds with long eyelashes, mild strabismus, small narrow nose, and narrow/tented upper vermillion. Brain MRI showed FLAIR hyperintensities in the pons.

Individual 7

This individual is the first child in a family of Slavic origin. He was born at 41 weeks of gestation by caesarean section due to breech position, birth weight 3180g (-1 SD), length 51 cm (-1 SD), head circumference 35 cm (-0.5 SD) and Apgar score 9/9. First adaptation was normal. He was first time evaluated at 4 ½ months due to hypotonia and suspicion of seizures. Additionally, he had gastro-esophageal reflux and poor weight gain. Abnormal facial phenotype was noticed. He had convergent strabismus, nystagmus. His psychomotor development was delayed. He started to walk at 21 months.

Assessment at 2 ½ years showed moderate developmental and speech delay, and normal growth. His speech corresponded to the age of eleven months. He has remarkably dysmorphic face with deeply set eyes, inner canthal folds, hypotelorism, convergent strabismus, nystagmus, short and upturned nose, hypoplastic alae nasi and full cheeks. His ears were large with simple morphology. His hair and skin were fair. He has 2-3 toe partial syndactyly. Brain MRI at age 5 months revealed mild dilation of lateral ventricles and thin corpus callosum. Renal ultrasound showed mild hydronephrosis in left side. Chromosomal microarray, genomic sequencing panel and extensive metabolic investigations (amino acids, organic acids, very long chain fatty acids, transferrin isoforms, glycosaminoglycans, oligosaccharide, and creatine/guanidinino-acetate) were normal.

Individual 8

Individual 8 was born to healthy unrelated parents of Mexican background. She was seen at 9 months of age at an outreach clinic due to hypotonia, dysmorphic facial features, and developmental delay. There had been an initial concern for Down syndrome, but a postnatal karyotype was 46 XX. On examination she was found to have metopic craniosynostosis, a flat midface, depressed nasal bridge, apparent telecanthus with proptosis and epicanthus inversus, a medial eyebrow flare, and moderate hypotonia. After the initial visit she was lost to follow up.

Figure S1.

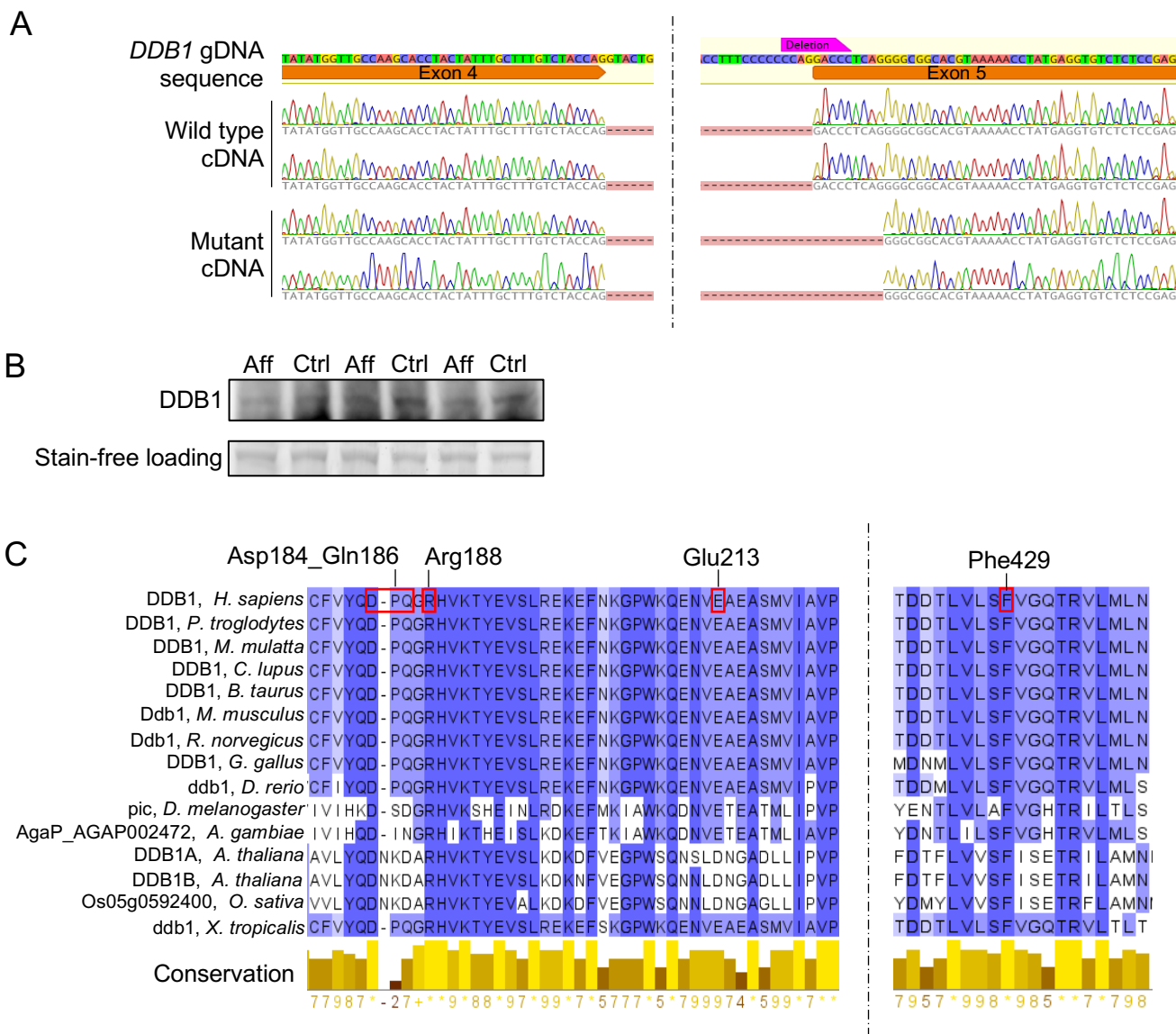


Figure S1. Effect of the DNA deletion in individual 1 on *DDB1* expression and protein sequence conservation of *DDB1* determined by homologous sequence alignment. (A) Sanger sequencing of cloned cDNA from individual 1 revealed a deletion of the first 9 nucleotides of exon 5 within the mutant allele, labelled “Mutant cDNA”. Individual 1 had one allele carrying g.61094361_61094369del, corresponding to 9 nucleotides spanning the intron 4-exon 5 boundary, depicted in the diagram by the pink arrow above the *DDB1* gDNA sequence. (B) Western blot analysis on total extracts from affected individual 1 (“Aff”) and control (“ctrl”) lymphoblast cells to assess total *DDB1* levels, which appear unchanged. (C) Protein alignment of *DDB1* homologues was performed to determine protein sequence conservation and regions of interest are shown. Residues impacted by variants within affected individuals in this study are highlighted in the *H. sapiens* track by red boxes and are labelled above accordingly. Higher scores in the conservation track indicate higher sequence similarity.

Figure S2

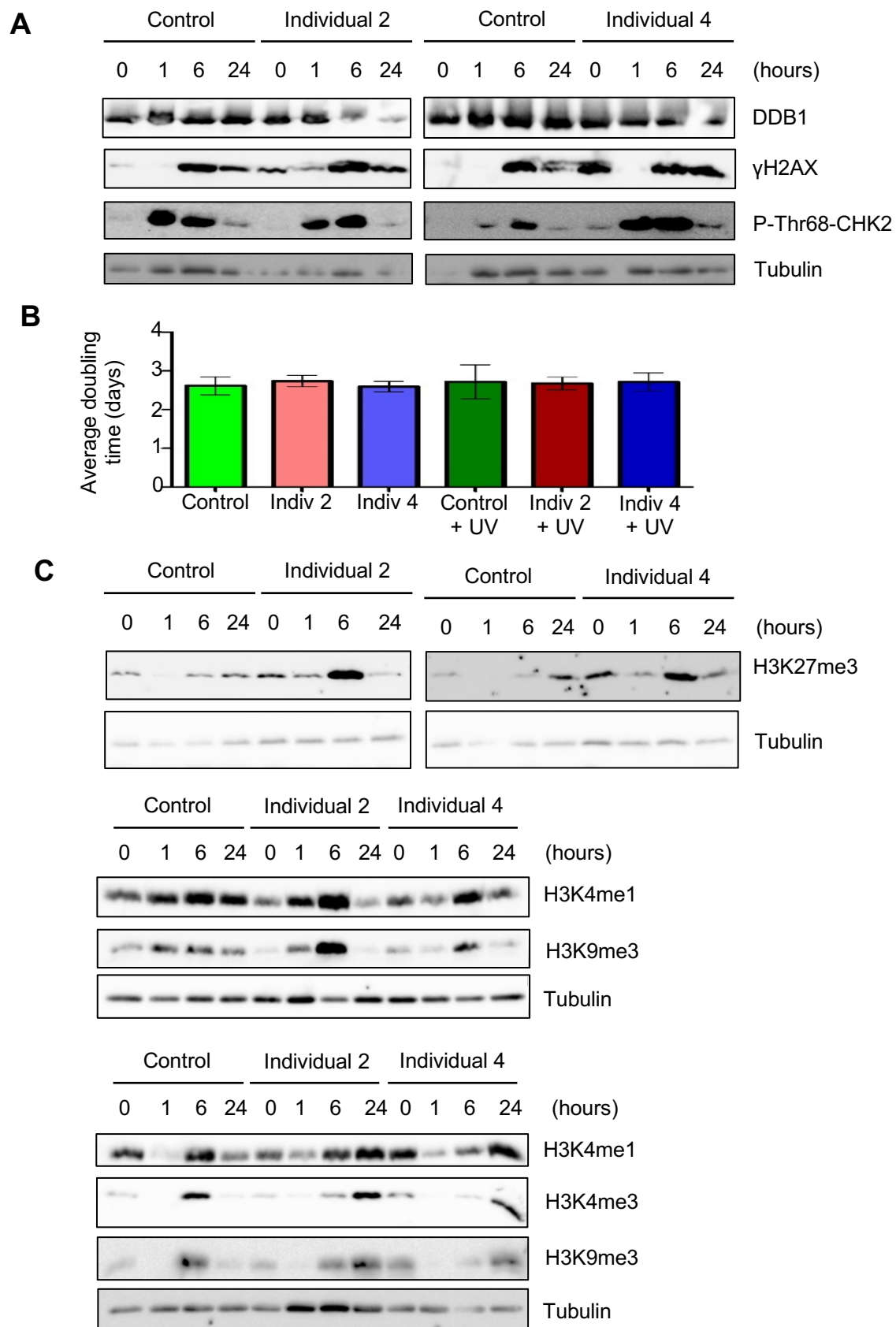


Figure S2. DNA damage signatures, proliferation rate, and histone methylation of lymphoblast cells following UV damage. (A) Another replicate of western blot analysis on total extracts from lymphoblast cells from control and affected individuals, from Fig. 3A. Untreated cells are shown at 0 h, whereas the other time intervals indicate the number of hours following UV exposure. Total DDB1 and the levels of γ H2AX and p-Thr68-CHK2 phosphorylation were assessed: again, DDB1 was found to be unchanged, γ H2AX and p-Thr68-CHK2 levels were induced as expected, p-Thr68-CHK2 generally to a higher level than controls, and γ H2AX increased to a similar level as controls but not elevated for as long after damage. (B) Cell proliferation of control and affected lymphoblast cells was measured by harvesting and counting cells on various days after initial plating, either with or without UV exposure, as depicted in Fig. 3C. For each of the three biological replicates, doubling time of the different cell lines with or without treatment was determined and these values were not determined to be statistically different using one-way ANOVA. Depicted error bars are standard error of the mean. (C) Additional replicates of western blot analysis from Fig. 3D using total extracts from control and affected lymphoblast cells. Untreated cells are shown at the 0 h time point, whereas the other time intervals indicate the number of hours following UV exposure. Levels of various histone H3 methylations were assessed and found to be abnormal in affected cells.

Table S1. Details of genomic sequencing for *DDB1* cohort

Individual	Capture Kit	Coverage	Sequencer and chemistry
Individual 1	Proprietary GeneDx	Mean depth of coverage 106X 98.4% sequence reads covered at least 10x	Illumina sequencer
Individual 2	Agilent CRE V1.0	Average coverage: 121, 154, 158x 96% of bases covered at least 20x	HiSeq 2500 2x100 chemistry
Individual 3	Exome BGI Exome kit 59M	Average coverage: 177, 169 and 181x 97% of bases covered at least 20x	BGISEQ
Individual 4	Illumina TruSeq Customized exome capture (37.5Mb)	Average coverage: 121x, 153x, 122x >95% of bases covered at 20x	Illumina HiSeq X
Individual 5	Agilent exome V6	Average coverage: 145X, 105X, 133X	Illumina NextSeq 550

		>96% of bases covered at 20X	
Individual 6	Whole-exome captured with NimbleGen SeqCap EZ v.3.0 rapid or v.4	Average coverage: 140.15 >97% of bases covered at 20x	Exome sequenced on a HiSeq 2500 or NovaSeq 6000 with the Kapa Biosystem's Library Preparation Kit
Individual 7	SureSelect V7	Average coverage: Proband: 90x Mother: 119x Father: 103x	NovaSeq 6000, 2x150 paired-end reads
Individual 8	SureSelectV5	Average coverage: 103x	HiSeq2500

Table S2. Additional variants from genomic sequencing considered for each individual. See separate excel file.

Table S3. In-silico predictions for *DDB1* variants

Variant g. (GRCh37/hg19;chr11) Variant c. (NM_001923.4) Variant p. (NP_001914.3)	Individual	gnomAD v.2.1.1 (allele freq- uency)	Conservation of residue (considering 100 species)	CADD PHRED score ¹	PolyPhen-2 score ²	SIFT score ³
c.551_559del p.(Asp184_Gln186del)	P1	absent	yes	N/A	N/A	N/A
g.61094353G>A c.562C>T p.(Arg188Trp)	P2	absent	yes	34	1	0
g.61094352C>T c.563G>A p.(Arg188Gln)	P3	absent	yes	35	1	0.005
g.61094278C>T c.637G>A p.(Glu213Lys)	P4, P5, P6 P7	absent	yes	34	1	0.008
g.61083980A>C	P8	absent	yes	28.8	0.999	0.001

c.1285T>G p.(Phe429Val)							
----------------------------	--	--	--	--	--	--	--

Table S4. Detailed phenotype information for individuals with *DDB1* variants.

Individual	P1	P2	P3	P4	P5	P6	P7	P8
Ethnicity	Caucasian	Ashkenazi Jewish	Turkish	Caucasian	Armenian	Caucasian	Caucasian	Mexican
Gender	Female	Female	Male	Female	Female	Male	Male	Female
Age at presentation	12 months	3y 10m	10y 8m	9 m	9y 9m	6m	4.5 months	1y
Age at last assessment	17 years	9y 2m	10y 8m	3y	13y	22m	2 years 11 months	1y
MOLECULAR DATA								
DDB1 variant (g) Hg19	chr11: 61094361_61094369del	chr11: 61094353G>A	chr11: 61094352C>T	chr11: 61094278C>T c.637G>A p.(Glu213Lys)				chr11:g. 61083980A>C
DDB1 variant (c) (NM001923.4) Variant (p) (NP_001914.3)	c.551_559del p.(Asp184_Gln186del)	c.562C>T p.(Arg188Trp)	c.563G>A p.(Arg188Gln)					c.1285T>G p.(Phe429Val)
BIRTH DETAILS								
Birth weight (g, gestation, centile)	2040 (38/40) <3 rd centile	2500 (40/40) (3-10 th centile)	4040 (42/40) (70th centile)	3480 (42/40) (70th centile)	2900 (36/40) (25-50 th centile)	2960 (38/40) (23rd centile)	3180 (41/40) (12th centile)	NR
Birth length (cm, centile)	47 (10 th centile)	49 (42nd centile)	54 (60th centile)	52 (93rd centile)	47 (50 th centile)	NR	51 (72 nd centile)	NR

Birth HC (cm, centile)		NR	37 (74th centile)	34.5 (60th centile)	NR	NR	35 (31st centile)	NR
Neonatal complications	Jaundice. Nasogastric tube feeding for one week	Hypoglycemia & tachypnea at birth, admitted to NICU for 1 month	Nil	Nil	Neonatal feeding difficulties and jaundice	Hypotonia, temperature instability, hypoglycemia, torticollis	nil	Hypotonia
Current weight (kg, age of measurement, centile)	80.3 kg; > 95th percentile (at age 16 years, 9 months) 88 kg @18y2m (97 th centile)	52.7 @9y 2m (>97th centile)	52.8 @ 10y 8m (>97th centile)	12.35 @3y (4th centile)	45.5 @13y 9m (25-50 th centile) BMI 23,55 (+1.85 SD)	13.05 @ 22 mo (82nd centile)	12.9 @2y 5m (36th centile)	NR
Current height (cm, centile, age of measurement)	150.4 cm @ 18y 2m (2nd percentile)	137 @9y 2m (75th centile)	138 @ 10y 8m (95th centile)	90 @ 3y (14th centile)	139 @13y 9m (<1 st centile)	87.6 @ 18m (98th centile)	86.2 @2y 5m (11th centile)	NR
Current HC (cm, centile, age of measurement)	NR	51 @9y 2m (50th centile)	53 @ 10y 8m (79th centile)	47 @3y (5th centile)	52.4 @13y 9m (10-25 th centile)	48.2 @18m (73rd centile)	49.7 @2y 5m (25 th centile)	NR
Malformations	Anterior anus with rectovaginal fistula	Accessory band across left ventricle of heart Horseshoe kidney Anterior ectopic anus	nil	nil	Horseshoe kidney with left vesico-ureteric reflux, pelvicalyceal dilatation kidney and megaureter	nil	Mild left hydronephrosis	Metopic cranio-synostosis
NEUROLOGICAL FEATURES								
Hypotonia	Moderate	Mild	nil	Moderate	Moderate	Moderate	Moderate	Moderate
Intellectual disability	Moderate	Moderate DD	Mild (IQ69)	Mild	Mild-moderate	Mild	Moderate DD	Moderate DD
Vision	Normal vision	Normal	Normal	Hypermetropia and strabismus	Esotropia, hypermetropia nystagmus	Strabismus	Convergent strabismus and nystagmus	Normal

Hearing	Normal	Bilateral hearing loss - wears aids	Normal	Conductive hearing loss requiring tympanostomy tubes	Normal	Normal	Normal	Normal
Seizures	No	No	No	No	No	Episodes of eye rolling & head movement; no confirmed seizures	No	No
Brain MRI	Mild ventriculomegaly	Thinning of posterior body of corpus callosum Non-specific abnormal signal in the genu of corpus callosum Ventriculomegaly	Not performed	Mild delayed myelination	Not performed	Bilateral linear T2 Flair hyperintensities in the central segmental tract of the pons	Mild dilation of lateral ventricles, thin corpus callosum	Not performed
CRANIOFACIAL FEATURES								
Eyebrows	Thick, light blonde	Prominent, straight and dark eyebrows with synophrys	Synophrys	Straight, dark, eyebrows with medial flare, lateral extension	Dark, straight, heavy eyebrows	Medial flare	Unremarkable	Medial flare
Eyes	Deep-set, upslanting palpebral fissures, epicanthic folds	Long palpebral fissures with lateral extension Epicanthus inversus Long dark eyelashes Striking blue irides	Small eyes	Lateral extension to palpebral fissures	Unremarkable	telecanthus, lateral extension to palpebral fissures epicanthal folds with long eyelashes	Deeply set eyes, inner canthal folds, hypotelorism, convergent strabismus, nystagmus	Apparent telecanthus with proptosis and epicanthus inversus
Nose	Short nose in early childhood	Short nose with small nares	Unremarkable	Short	Unremarkable	Small narrow nose with	Small and upturned nose,	Depressed nasal bridge

		Hypoplastic alae nasi Narrow base High nasal bridge				narrow alae nasi	hypoplastic alae nasi	
Midface	Very round cheeks	Mid-face hypoplasia	Unremarkable	Mid-face hypoplasia	Round face; mild midface hypoplasia; full cheeks	Unremarkable	full cheeks	Mid-face hypoplasia
Mouth	Thin upper vermillion border, wide mouth	Unremarkable	Unremarkable	Thin upper vermillion border	Protruding upper lip, thin vermillion border, maxillary overbite, asymmetric occlusion of teeth	Ankyloglossia (underwent frenotomy); retrognathia; narrow, tented lip	Unremarkable	Unremarkable
Ears	Large ears with large and long ear lobes	Low-set & large ears with long fleshy lobes	Large earlobes	Large ears with fleshy lobes	Large fleshy ears and earlobes	Low set and fleshy ears	Large ears with simple morphology	Unremarkable
Neck	Short neck with excess skin at base of neck (posterior thickening)	Short	Unremarkable	Short	Short	Torticollis	Unremarkable	Unremarkable
OTHER PHENOTYPIC FEATURES								
Skin	Fair	Hirsutism on back. Fibro-fatty deposition on the lateral dorsal aspect of the torso with thickened overlying skin	Unremarkable	Soft skin	Hirsutism	Integumentary papules on chin	Mild cutis laxa	Unremarkable
Joints	Joint laxity	Hirsutism on back. Fibro-fatty deposition on the lateral dorsal	Unremarkable	Soft skin	Hirsutism	Integumentary papules on chin	Mild cutis laxa	Unremarkable

		aspect of the torso with thickened overlying skin						
Hands and feet	Very small hands and feet Fourth metacarpal shortening bilaterally, brachydactyly	Significant cutaneous syndactyly of 2-3 toes Brachydactyly Tapering fingers	Short toes	Short toes	Short toes	NR	2-3 toe partial syndactyly	NR
Other	ADHD and anxiety requiring medication Hypothyroidism Recurrent otitis media	Nasal voice with some articulation difficulties Marked truncal obesity	Frequent otitis media	Obstructive sleep apnoea requiring adenotonsillectomy @ 2 y 9m	NR	NR	Gastro-esophageal reflux	NR

Materials and Methods

Clinical recruitment

Eight independent families presented to Medical Genetics or Child Neurology Services (Portland, USA; Ontario, Canada; Düsseldorf, Germany; Melbourne, Australia; Utrecht, Netherlands; New York, USA; Tartu, Estonia; and Philadelphia, USA) for evaluation of children with apparent syndromic intellectual disability. Each underwent exome or genome sequencing to identify the molecular etiology of their condition. Research protocols were approved in each country via institutional research boards and regional ethics committees, in keeping with national guidelines and the principles laid out in the Declaration of Helsinki and informed consent was obtained from all participants.

Exome sequencing and variant validation

Affected individuals underwent exome sequencing in eight different genomic sequencing laboratories. Genomic DNA was extracted from whole blood from the affected children and their parents. Exome sequencing was performed with a variety of standard capture kits according to manufacturer's instructions. For each family, parentage was confirmed by analysis of inherited variants in the sequencing data. Sanger sequencing was used to validate *DDB1* variants identified by sequencing.

Protein sequence conservation analysis

Homologues of human *DDB1* were identified using the NCBI database HomoloGene.⁴ JalView was then used to generate multiple sequence alignments of these protein

sequences using the MUSCLE algorithm, as well as to determine conservation for each position of the alignment using AMAS scoring.⁵⁻⁷

Real-time PCR

Immortalized lymphoblast cell lines from affected individuals were established from blood samples at The Centre for Applied Genomics (Toronto, Canada). Total RNA was obtained from affected and control lymphoblast cell lines with the RNeasyMinikit (QIAGEN) and reverse transcribed into complementary DNA (cDNA) with iScript kit (BioRad Laboratories) according to manufacturer's instructions. Control reactions without reverse transcriptase were prepared in parallel. cDNA was amplified with gene-specific primers and iQ SYBR Green mastermix under the following conditions: 35 cycles of 95°C for 10 s, 55°C for 20 s, 72°C for 30 s, and a final melting curve generated in increments of 0.5°C per plate read on a CFX96 Touch Real-time PCR Detection System (BioRad Laboratories). Gene expression was quantified using the standard Ct method with CFX software (BioRad Laboratories), and all data corrected against *GAPDH* as an internal control. Primer sequences available upon request.

Splicing analysis

Total RNA was obtained from the affected lymphoblast cell line of interest and reverse transcribed into cDNA as above. cDNA was amplified with GoTaq DNA Polymerase and primers to span specific exons. PCR reactions were then purified using the QIAquick PCR Purification Kit (QIAGEN) before being used for TOPO TA cloning (Thermo Fisher Scientific). Transformed clones were isolated and cultured. Plasmid DNA was isolated using the

QIAprep Spin Miniprep Kit (QIAGEN), which was then used for Sanger sequencing to determine the inserted cDNA sequence.

Western blot analysis

Western blot analysis was conducted to assess protein levels in lymphoblast cells from affected individuals. Cells were lysed in radioimmunoprecipitation assay buffer containing 10 mg/mL each of aprotinin, phenylmethanesulfonyl fluoride, and leupeptin (all from Sigma) for 20 min at 4°C, followed by centrifugation at 13,000xg for 15 min and retrieval of supernatants. Total protein concentrations were determined by Bradford protein assay (BioRad Laboratories). Protein samples were resolved by SDS-PAGE, transferred onto nitrocellulose membrane and incubated in blocking solution [tris-buffered saline (TBS), 5% non-fat milk, 0.05% Tween-20] for 1 h at room temperature followed by overnight incubation with primary antibody at 4°C (DDB1, Abcam ab97522; phospho-histone H2AX (Ser139; γ H2AX), Sigma-Aldrich 05-636; phospho-Chk2 (Thr68), Cell Signaling 2197; β -Tubulin, Abcam ab6046; H3K4me1, Abcam ab8895; H3K4me3, Abcam ab8580; H3K9me3, Abcam ab195497; H3K27me3, Sigma-Aldrich 07-449). Membranes were washed with TBS and 0.1% Tween-20 three times followed by incubation with secondary antibody (HRP conjugated anti-rabbit or anti-mouse; BioRad Laboratories) for 1 h at room temperature. Blots were visualized by autoradiography using the Clarity Western ECL substrate (BioRad Laboratories). When necessary, membranes were stripped using Restore PLUS Western Stripping Buffer (Thermo Scientific) according to the manufacturer's instructions. Control protein was extracted from control cell lines from healthy, unrelated, age-matched individuals. All western blots were conducted in multiple biological replicates and representative images are displayed.

Proliferation assay

Lymphoblast cells were plated at a density of 10^5 cells/mL/well in 24 well dishes. At the appropriate time interval after plating and applicable treatment, cells were harvested and counted using the Countess Automated Cell Counter (Invitrogen). For each of the three biological replicates, the exponential growth nonlinear regression equation was used to determine the doubling time of the different cell lines, which were then compared using one-way ANOVA.

UV treatment

Lymphoblast cells were treated with 75 J/m^2 UV using the FB-UVXL-1000 UV Crosslinker (Fisher Scientific). After the appropriate time intervals following treatment, cells were harvested and used for subsequent analysis.

Facial analysis

An average face was generated while allowing for asymmetry preservation and equal representation by individuals using previously published methods.⁸

Supplemental References

1. Kircher, M., Witten, D.M., Jain, P., O'Roak, B.B., Cooper, G.M., and Shendure, J. (2014). A general framework for estimating the relative pathogenicity of human genetic variants. *Nat Genet.* *46*, 310-5.
2. Sunyaev, S., Vasily, R., Koch, I., Lathe 3rd, W., Kondrashov, A.S., and Bork, P. (2001).

Prediction of deleterious human alleles. *Hum Mol Genet* 10, 591-597.

3. Ng, P., and Henikoff, S. (2003). SIFT: predicting amino acid changes that affect protein function. *Nucleic Acids Res.* 31, 3812-3814.
4. NCBI Resource Co-ordinators. (2018). Database resources of the National Center for Biotechnology. *Nucleic Acids Res.* 46, D8-D13.
5. Edgar RC. (2004). MUSCLE: multiple sequence alignment with high accuracy and high throughput. *Nucleic Acids Res.* 32, 1792-7.
6. Waterhouse, A. M., Procter, J. B., Martin, D. M., Clamp, M., & Barton, G. J. (2009). Jalview Version 2--a multiple sequence alignment editor and analysis workbench. *Bioinformatics (Oxford, England)*, 25, 1189–1191.
7. Livingstone, C. D., & Barton, G. J. (1993). Protein sequence alignments: a strategy for the hierarchical analysis of residue conservation. *Computer applications in the biosciences: CABIOS*, 9, 745–756.
8. Reijnders, M., Miller, K. A., Alvi, M., Goos, J., Lees, M. M., de Burca, A., Henderson, A., Kraus, A., Mikat, B., de Vries, B., Isidor, B., Kerr, B., Marcelis, C., Schluth-Bolard, C., Deshpande, C., Ruivenkamp, C., Wieczorek, D., Deciphering Developmental Disorders Study, Baralle, D., Blair, E. M., et al., (2018). De Novo and Inherited Loss-of-Function Variants in TLK2: Clinical and Genotype-Phenotype Evaluation of a Distinct Neurodevelopmental Disorder. *Am. J. Hum. Genet.* 102, 1195–1203.